1-1-2018

Super-resolution in the presence of atmospheric optical turbulence

Russell C. Hardie
University of Dayton, rhardie1@udayton.edu

Michael A. Rucci
Air Force Research Laboratory

Barry K. Karch
Air Force Research Laboratory

Alex J. Dapore

Douglas R. Droege

eCommons Citation

Russell C. Hardie, Michael A. Rucci, Barry K. Karch, Alex J. Dapore, Douglas R. Droege, "Super-resolution in the presence of atmospheric optical turbulence," Proc. SPIE 10650, Long-Range Imaging III, 106500H (11 May 2018); https://doi.org/10.1117/12.2303657

Super-resolution in the presence of atmospheric optical turbulence

Russell C. Hardie*[a], Michael A. Rucci[b], Barry K. Karch[b], Alexander J. Dapore[c], and Douglas R. Droege[c]

[a]Department of Electrical and Computer Engineering, University of Dayton, 300 College Park

[b]Air Force Research Laboratory, 2241 Avionics Circle, Wright Patterson AFB, OH 45433

[c]L-3 Cincinnati Electronics, 7500 Innovation Way, Mason, Ohio 45040

ABSTRACT

The design of imaging systems involves navigating a complex trade space. As a result, many imaging systems employ focal plane arrays with a detector pitch that is insufficient to meet the Nyquist sampling criterion under diffraction-limited imaging conditions. This undersampling may result in aliasing artifacts and prevent the imaging system from achieving the full resolution afforded by the optics. Another potential source of image degradation, especially for long-range imaging, is atmospheric optical turbulence. Optical turbulence gives rise to spatially and temporally varying image blur and warping from fluctuations in the index of refraction along with optical path. Under heavy turbulence, the blurring from the turbulence acts as an anti-aliasing filter, and undersampling does not generally occur. However, under light to moderate turbulence, many imaging systems will exhibit both aliasing artifacts and turbulence degradation. Few papers in the literature have analyzed or addressed both of these degradations together. In this paper, we provide a novel analysis of undersampling in the presence of optical turbulence. Specifically, we provide an optical transfer function analysis that illustrates regimes where aliasing and turbulence are both present, and where they are not. We also propose and evaluate a super-resolution (SR) method for combating aliasing that offers robustness to optical turbulence. The method has a tuning parameter that allows it to transition from traditional diffraction-limited SR, to pure turbulence mitigation with no SR. The proposed method is based on Fusion of Interpolated Frames (FIF) SR, recently proposed by two of the current authors. We quantitatively evaluate the SR method with varying levels of optical turbulence using simulated sequences. We also presented results using real infrared imagery.

Keywords: super-resolution, long range imaging, infrared imaging, atmospheric turbulence, optical turbulence, image restoration.

1. INTRODUCTION

Multi-frame image restoration has proven to be a particularly powerful tool for atmospheric optical turbulence mitigation (TM)[1-3]. Furthermore, multi-frame super-resolution (SR) algorithms are effective for aliasing reduction and resolution enhancement for detector limited systems[4-9]. However, rarely are TM and SR addressed simultaneously[10-13]. With no turbulence, many image systems are undersampled because of design choices in the trade space[6,14]. Here, traditional SR methods may be applied. Under heavy turbulence, the turbulence optical transfer function (OTF) acts as a low pass anti-aliasing filter, preventing aliasing. This makes SR unnecessary, but TM is critical. However, in the case of mild to moderate turbulence, we show that imaging systems may have both undersampling and turbulence degradations. In such cases, addressing TM and SR jointly is desired[10-13]. This requires a flexible multi-frame image restoration algorithm. We believe that an excellent choice for this purpose is Fusion of Interpolated Frames (FIF) SR method, recently proposed by Karch and Hardie[9].

The FIF SR method[9] is a multi-frame image restoration and SR algorithm that applies single frame interpolation to each low resolution (LR) input frame up to the Nyquist sampling grid (as defined by the optical cut-off frequency). The interpolated frames are then fused using specially designed weights that may depend on subpixel alignment for each interpolated pixel, color information (if present), and local motion analysis. Finally, the FIF SR method uses a Wiener filter to provide restoration for the OTF blurring model.

Here we extend the FIF SR approach to allow it to effectively treat SR and TM simultaneously. To do so, we make two important new modifications to the OTF model used by the Wiener filter. The first modification is to incorporate an atmospheric OTF model, in addition to modeling the optical system[9]. For the atmospheric OTF, we use the innovative approach of incorporating the estimated level of short-exposure registration into the model, as described by Hardie et al[1].

Long-Range Imaging III, edited by Eric J. Kelmelis, Proc. of SPIE Vol. 10650, 106500H
 · doi: 10.1117/12.2303657

This allows the Wiener filter to be better tuned to the level of blurring in the fused image prior to restoration. Another key modification of our extended FIF SR method is that we set the subpixel fusion weighting parameter according to the level of turbulence. Under light turbulence, we use a subpixel fusion weighting that gives a large weight only to pixels that lie very close to the high resolution grid. This provides maximum SR and minimum interpolation blurring. It also provides less temporal averaging. Under heavy turbulence, more temporal frame averaging is needed and the subpixel weight is set to be less selective. However, being less selective, and giving significant weight to pixels with larger interpolation error, increases burring in the fused image. While this seems undesirable, it may be necessary to provide enough temporal averaging to combat the turbulence. To address the increased interpolation blurring we introduce a new interpolation blurring OTF component in the overall OTF model. This allows the Wiener filter to smartly correct for the specific level of interpolation blurring introduced in the interpolation step of the algorithm, in addition to the other OTF components.

The remainder of this paper is organized as follows. In Section 2, we describe the FIF SR method. In Section 3, we introduce the OTF model used by the FIF SR method that incorporates diffraction, turbulence, and interpolation blurring. Simulation results are presented in Section 4 to illustrate the efficacy of the new method. Finally, we offer conclusions in Section 5.

2. FUSION OF INTERPOLATED FRAMES SUPER-RESOLUTION

The FIF SR method[9] is summarized in the block diagram in Fig. 1. Short exposure LR observed frames are registered using a robust global affine model. Global tilt components of the turbulence, as well as camera motion, are accounted for with this model. Accounting for local warping from turbulence requires optical flow estimation[1] and is not included in this work. Since our focus here is on light to moderate turbulence, where TM and SR are accomplished jointly, we find that useful results can be obtained with a global motion model. We also only consider single band imagery here. Next, the registered frames are interpolated to a pixel spacing at the Nyquist sampling rate, as defined by the optical cut-off frequency for the diffraction limited optics. We use bicubic interpolation here for this purpose.

The heart of the FIF SR method is the fusion of the interpolated frames. Let interpolated pixel i in frame k be denoted $f_k(i)$, and fused pixel i on the Nyquist grid be $g(i)$. Given K input frames, the FIF SR output may be expressed as

$$g(i) = \frac{\sum_{k=1}^{K} w_{i,k}(\beta) f_k(i)}{\sum_{k=1}^{K} w_{i,k}(\beta)}, \tag{1}$$

where

$$w_{i,k}(\beta) = e^{-\left(d_x(i,k)^2 + d_y(i,k)^2\right)/\beta^2}, \tag{2}$$

is the sub-pixel interpolation weighting function with parameter β. This weight is governed by the distance between the i'th position on the Nyquist grid and the nearest un-interpolated observed pixel from Frame k, as shown in Fig. 2. The horizontal and vertical subpixel distances are respectively represented by $d_x(i,k)$ and $d_y(i,k)$ in Eq. 2.

Note that Eq. 2 gives a Gaussian weighting that is inversely proportional to the distance. Larger distances here implies a larger interpolation error. Thus, for larger distances a reduced weight is given to Frame k for computing SR Pixel i. The weighing function is plotted in Fig. 3 for β=0.1 and β=0.25. Note that, the larger the β, the larger the weight for a given distance. This makes the fusion less selective. When $\beta = \infty$, the fusion is simply a temporal average, with equal weight given to all frames (i.e., no selectivity). As β is reduced, the fusion is more selective, giving significant weight only to interpolated pixels that are close to their frame's native samples (less interpolation error). A small β gives the best SR results with minimum interpolation blurring. A larger β sacrifices resolution for more temporal averaging. The increased temporal averaging is needed to stabilize the warping and blurring in moderate to high turbulence, to give a fused image that appears to have a spatially invariant blurring and the correct geometry[1-3]. The tunability of the FIF SR method makes

it very powerful and practical for SR, especially SR in the presence of turbulence. Note that FIF SR is a type of non-uniform interpolation SR method[4,5,7]. The β parameter, however, sets it apart by giving it important flexibility. By fusing interpolated frames, the output will never be "missing" any pixels on the SR grid, as is the case with binning methods that populate an SR grid using the nearest observed pixel[5,7]. However, with a small β, FIF SR approaches a binning method (but without the danger of leaving empty bins).

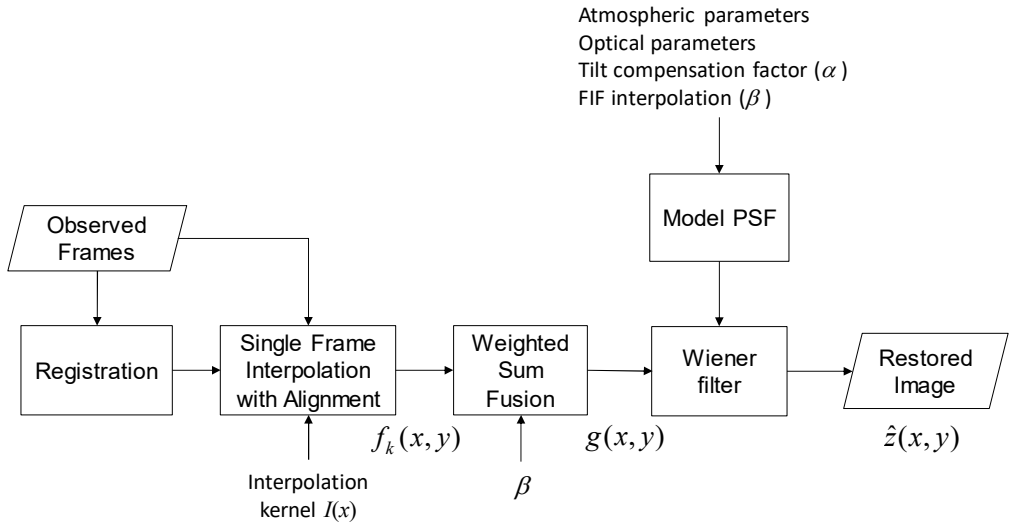

Figure 1. Block diagram of the FIF SR method. Observed frames are registered, interpolated individually, and then fused based on a special weighting function. A Wiener filter is used to provide restoration based on an OTF model that incorporates the level of registration accuracy, defined by α, and the subpixel weighting parameter, β.

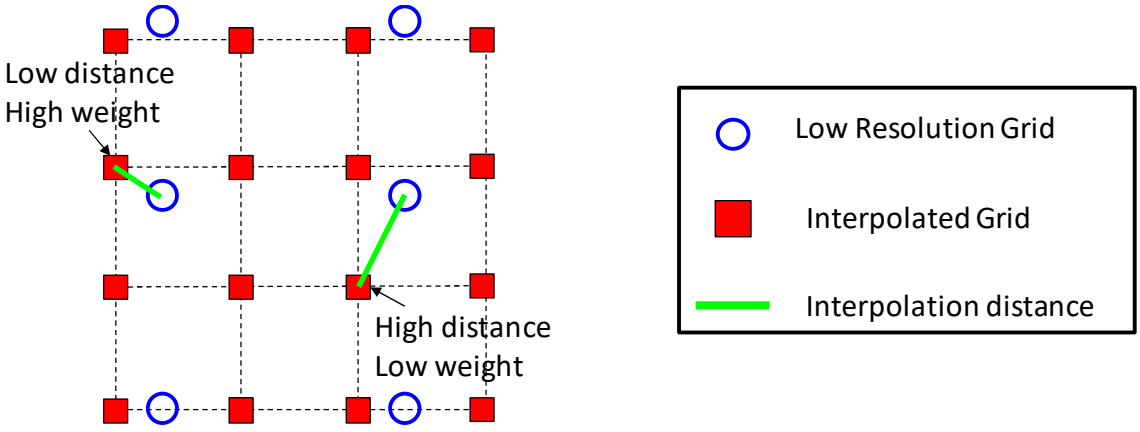

Figure 2. Illustration of the distances between the Nyquist interpolation grid (red squares) and the un-interpolated pixels from a given frame k (blue circles). A larger distance implies a larger interpolation error for that frame at that pixel, and consequently gets a lower weight using Eq. 2.

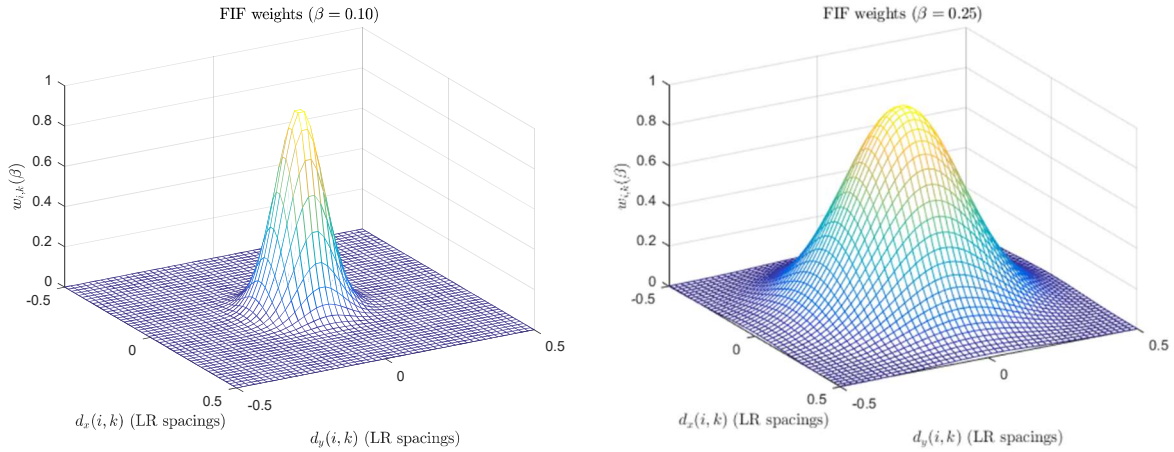

Figure 3. Fusion weighting functions from based on interpolation distance in Eq. 2 for β=0.1 (left) and β=0.25 (right). The larger the β, the larger the weight for a given interpolation distance, and the less selective the fusion.

Another important way to understand the tuning parameter β is to consider what we term the temporal "averaging power factor" of the fusion. By this, we mean the variance reduction factor for independent and identically distributed (i.i.d.) temporal samples, relative to a standard average. An averaging power factor of 1 means that the fusion provides the same variance reduction as a standard average (i.e., variance reduction of $1/K$). The averaging power factor for the FIF SR fusion can be shown to be

$$P_i(\beta) = \frac{\left(\sum_{k=1}^{K} w_{i,k}(\beta)\right)^2}{K\sum_{k=1}^{K} w_{i,k}^2(\beta)}. \tag{3}$$

If we assume uniform subpixel distances and a large number of input frames, it can be shown that the averaging power factor approaches the following for all pixels

$$P(\beta) = \frac{\left(\int_{x=-0.5}^{0.5}\int_{y=-0.5}^{0.5} e^{-\left(x^2+y^2\right)/\beta^2}\,dydx\right)^2}{\left(\int_{x=-0.5}^{0.5}\int_{y=-0.5}^{0.5}\left(e^{-\left(x^2+y^2\right)/\beta^2}\right)^2 dydx\right)}. \tag{4}$$

The averaging power factor in Eq. 4 is plotted in Fig. 4 as a function of β. Note that smaller values of β produce a smaller averaging power as a result of the greater selectivity. Understanding this gives us better insight for selecting β for FIF SR, especially in the presence of turbulence, where averaging power needed.

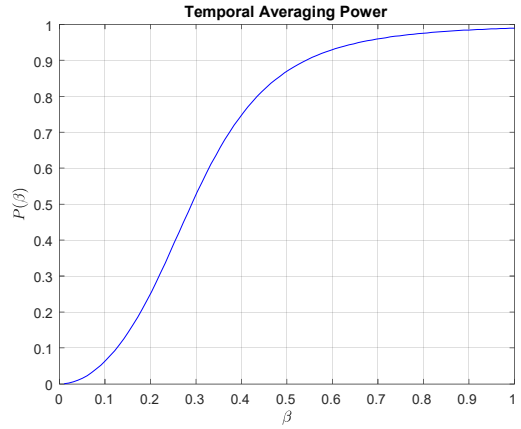

Figure 4. Averaging power factor from Eq. 4 as a function of β. An averaging power of 1 means the same variance reduction as a standard average (i.e., $1/K$).

3. OPTICAL TRANFER FUNCTION MODEL

The OTF model we use here for the FIF SR restoration includes diffraction, detector integration, the atmospheric turbulence, and blurring from the interpolation process itself. The diffraction, detector integration, and atmospheric components are modeled as follows

$$H_{\alpha}(u,v) = H_{\text{dif}}(u,v)H_{\text{det}}(u,v)H_{\text{atm},\alpha}(u,v), \tag{5}$$

where $H_{\text{dif}}(u,v)$ is the diffraction limited OTF of the optics, $H_{\text{det}}(u,v)$ is the detector OTF, and $H_{\text{atm},\alpha}(u,v)$ is the atmospheric OTF. The diffraction limited OTF for an optical system with a circular exit pupil is given by[15]

$$H_{\text{dif}}(\rho) = \begin{cases} \dfrac{2}{\pi}\left[\cos^{-1}\left(\dfrac{\rho}{2\rho_c}\right) - \dfrac{\rho}{2\rho_c}\sqrt{1-\left(\dfrac{\rho}{2\rho_c}\right)^2}\right] & \rho \le \rho_c \\ 0 & \text{otherwise} \end{cases} \tag{6}$$

where $\rho = \sqrt{u^2+v^2}$, $\rho_c = 1/(\lambda N)$ is the spatial cut-off frequency, λ is the wavelength, and N is the f-number of the optics. The detector OTF is the Fourier transform of the detector active area shape[6]. The atmospheric turbulence model we use is based on that described by Hardie et al[1,16]

$$H_{\text{atm},\alpha}(\rho) = \exp\left\{-3.44\left(\frac{\lambda l \rho}{r_0}\right)^{5/3}\left[1-\alpha\left(\frac{\lambda l \rho}{D}\right)^{1/3}\right]\right\}, \tag{7)14}$$

where l is the focal length, D is the aperture diameter, and r_0 is the Fried parameter. The parameter α is treated as the tilt reduction factor resulting from the registration step[1]. A value of α=0 is used with no registration (i.e., the long exposure OTF[16]), and a value of α=1 is used for ideal registration (i.e., the short exposure OTF[16]). This parameter must be estimated based on the turbulence level and the type of registration used. The diffraction and atmospheric point spread function (PSF) is then given by the inverse Fourier Transform

$$h_\alpha(x,y) = FT^{-1}\left\{H_\alpha(u,v)\right\}. \tag{8}$$

The camera model used in the simulation section is comprised of the parameters outlined in Table 1. Four OTF plots are shown in Fig. 5. The baseline system OTF without any turbulence OTF's is shown in Fig. 5a while Fig. 5b shows the system OTF with light turbulence. The light turbulence does not reduce the cutoff frequency of the system but does add some light blurring and spatially varying warp to the imagery. Moderate to heavy turbulence shown in Fig. 5c-d, respectively, leads to the turbulence reducing the modulation depth the spatial frequencies in the OTF. The increase in turbulence acts as an anti-aliasing low pass filter eliminating higher spatial frequencies past the folding frequency of the detector, as shown in the heavy turbulence case.

Table 1: Optical parameters for simulated data.

Parameter	Value
Aperture	D = 132 mm
Focal length	l = 770mm
F-number	$f/\#$ = 5.8
Wavelength	λ = 0.787 µm
Spatial cut-off freq	ρ_c = 218.3803 cyc/mm
Object distance	L = 7 km
Pixel Pitch	d_p = 6.5µm

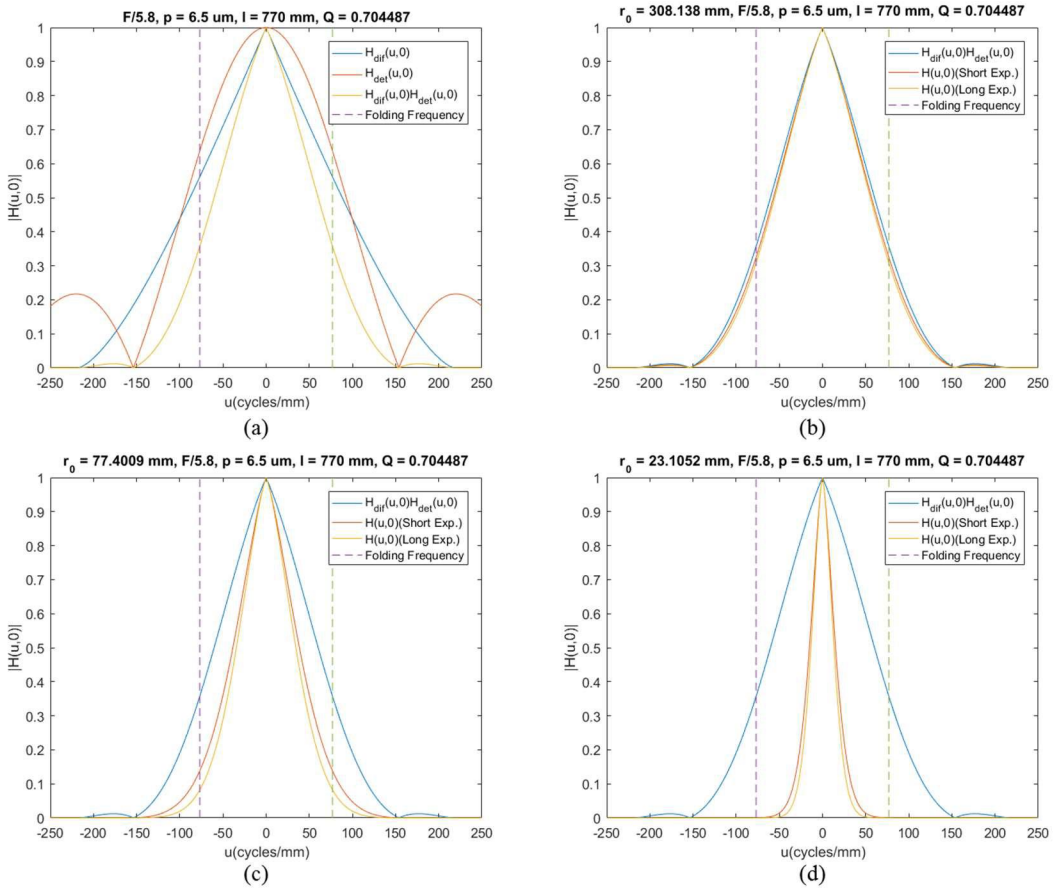

Figure 5. OTF plots including diffraction, detector, and turbulence for the three levels of turbulence. The imaging system components and subsequent system OTF is show in (a), while the system OTF with turbulence over the 7km horizontal path is calculated for (b) C_n^2 = 0.1e-15, (c) C_n^2 = 0.9e-15, (d) C_n^2 = 7.5e-15.

The new blurring component we consider here is that of the interpolation step. Assuming many input frames and uniform shifts at the subpixel level (after removing any integer pixel shifts), it can be shown that the temporally averaged interpolated frames experience a separable blurring with the following impulse response

$$h_\beta(x) = I(x) \sum_{k=-\infty}^{\infty} \mathrm{e}^{-(x-k)^2/\beta^2} \,\mathrm{rect}\left(x-k\right). \tag{9}$$

The interpolation function used is designated here as $I(x)$. The 2D impulse response would be given by

$$h_\beta(x,y) = h_\beta(x) h_\beta(y). \tag{10}$$

This blurring impulse response is plotting Fig. 6 for three different values of β, a cubic interpolation function, and an upsampling factor of L=4. Note that for a large β, the blurring impulse response matches the cubic interpolation kernel. For smaller β the interpolation blurring approaches a delta function (i.e., no blurring).

Combining all of the blurring components, we model the fused image in Fig. 1 as

$$g(x,y) = z(x,y) * h(x,y), \tag{11}$$

where $z(x,y)$ is the ideal image and

$$h(x,y) = h_\alpha(x,y) * h_\beta(x,y). \tag{12}$$

The Wiener filter in the FIF SR method is designed to provide deconvolution of the overall blurring impulse response in Eq. 12. It is interesting to note that the Wiener filter is being used to not only compensate for the turbulence and optics, but is also tuned to the level of registration (with α) and the level of interpolation blurring (with β) from the preceding steps of the processing algorithm itself. We believe this innovation allows it to provide a better estimate of the true image.

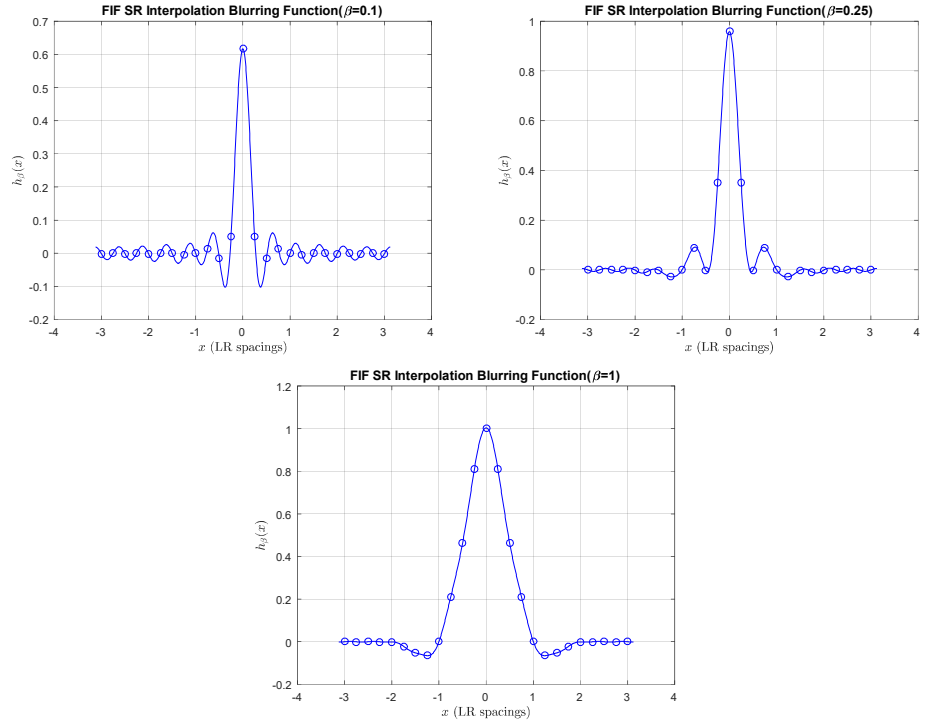

Figure 6. Interpolation blurring impulse response from Eq. 9 using a cubic interpolation function for $I(x)$ and upsampling factor of L=4 for three values of β. The discrete locations marked with circles are the impulse-invariant discrete impulse response samples.

4. SIMULATION RESULTS

To demonstrate the efficacy of the FIF SR method with both undersampling and turbulence, we have conducted a number of simulations using the anisoplanatic optical turbulence simulation tool recently developed by one of the authors[17]. Our simulation is novel in that we have included downsampling to simulate an undersampled imaging system. The parameters used in the simulation include the optical system parameters listed above in Table 1, along with the parameters outlined in Table 2.

Table 2: Parameters in simulation to generate observed frames.

Parameter	**Value**
Path length	L = 7 km
Propagation step	Δz = 700 m
Cropped screen samples	N = 448
Propagation screen width	X = 0.0035m
Number of phase screens	N = 10 (9 non-zero)
Phase screen type	Modified Von Karman with subharmonics
Inner scale	l_o = 0.01m
Outer scale	L_o = 300m
Image size (object plane)	9.2716 × 9.2716m
Image size (pixels)	448 × 448 pixels
Pixel skip	4 pixels (65 × 65 PSF array)
Input image dynamic range	256 digital units
Downsample Factor	4
Gaussian noise variance	9 digital units

The simulation was set up for a horizontal imaging case over seven kilometers. Three varying levels of turbulence were simulated to vary the amount of aliasing in the observed imagery. Turbulence C_n^2 strengths were set to 0.1e-15 (light turbulence), 0.9e-15 (medium turbulence), and 7.5e-15(heavy turbulence). It is important to remember that the heavy turbulence case used in this simulation provides an imaging scenario that has the camera turbulence-limited per Figure 1. Longer wavelengths with a similar optical system would require stronger turbulence strengths to achieve the same result of being turbulence-limited with no aliasing. Turbulent frames are convolved with the detector PSF and then downsampled by a factor of 4 to create the low resolution sampled frame. Translation shift is also added to the imagery to emulate camera jitter motion. Gaussian noise is introduced to the randomly translated low res sampled frame to create the final observed frame. Error metrics are computed between the true frame and the FIF SR output frame in the form of structural similarity (SSIM) and mean absolute error (MAE).

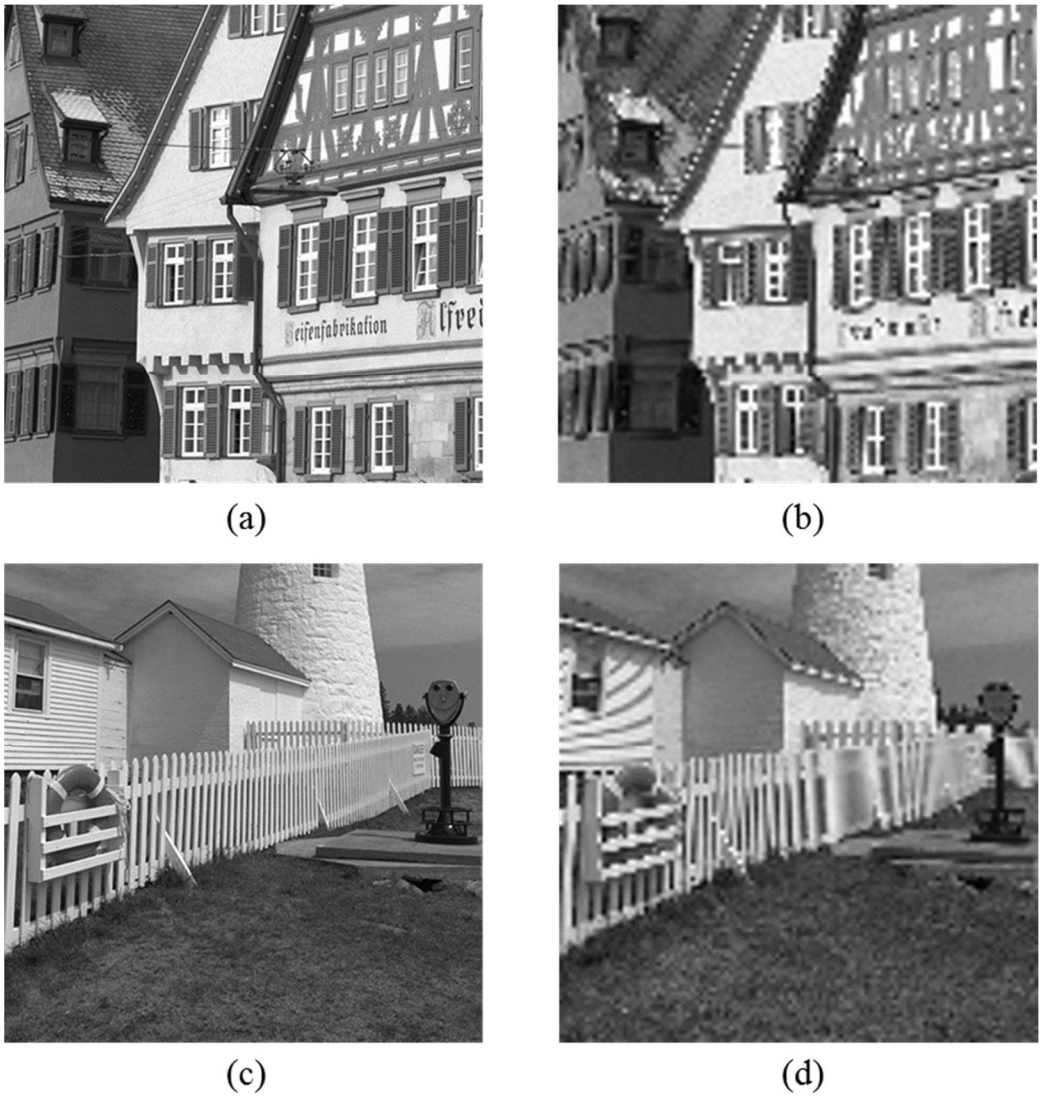

Figure 7. The truth frames used in the simulation are shown in subfigures (a) and (c). A purely downsampled image with L=4 for the corresponding truth images are shown in (b) and (d). The aliased images were interpolated back up to the native truth frame size using a bilinear interpolation.

The FIF SR method has been used to process an observed image sequence of 100 frames to produce a final output image. The truth images used for the simulation are shown in Fig. 7. These images show an aliased frame that is only downsampled with no additional blurring added from the system or turbulence PSF. A sample observed frame for the baseline system with and without varying levels of turbulence is displayed in Fig. 8. The short exposure turbulent frames illustrate the large amount of spatially varying warp and blur present in the simulated imagery. The anisoplanatic effects properly strengthen as the level of turbulence is increased for the simulation. Noise has also been added to the imagery shown in Fig. 8 to complete the simulation.

The FIF algorithm processed each simulated dataset multiple times, varying the strength of the averaging power factor, β, along with the tilt reduction factor, α, in generating the PSF model. PSF. Fried's parameter, r_0 , in Eq. (7), was given to the deconvolution kernel to ensure the proper atmospheric PSF was being applied in the final result. It is possible to try and estimate Fried's parameter and supply it to the algorithm. Finally, the noise-to-signal ratio (NSR) was optimized to yield the best Structural Similarity Index (SSIM) value.

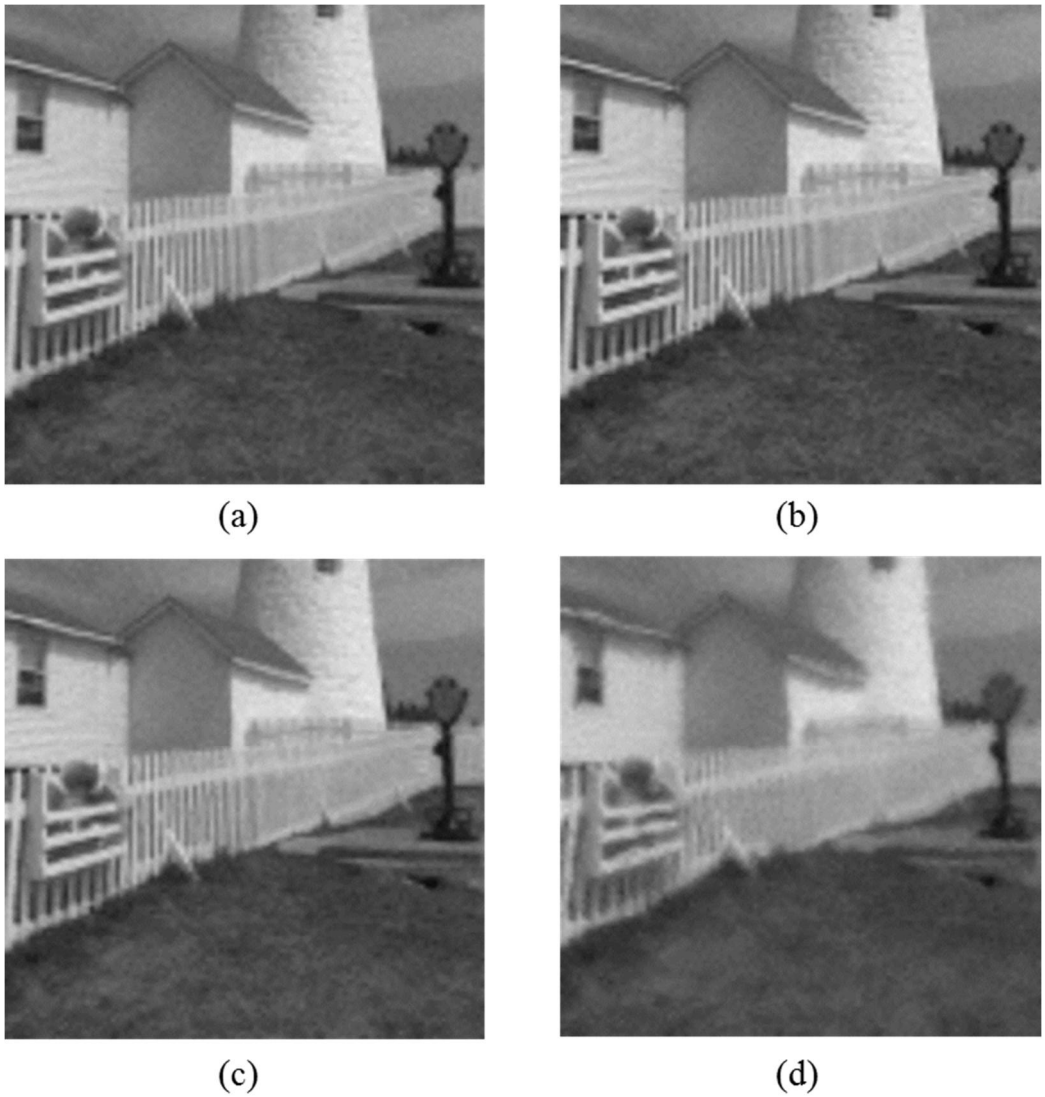

Figure 8. The four varying short exposure observed images with varying levels of turbulence. The top right image (a) has no turbulence at all as a baseline comparison. The rest have varying turbulence; (b) C_n^2 = 0.1e-15, (c) C_n^2 = 0.9e-15, (d) C_n^2 = 7.5e-15.

The corresponding observed and processed frames of the lighthouse image set are shown in Figs. 8 and 9, respectively. The additional processed frames of the houses are shown in Fig. 10. Note that higher levels of turbulence in Fig. 8 removes the effects of aliasing on the side of the house and the fence posts. The strongest turbulence case clearly removes a large amount of spatial frequency content in the image and amplifies the anisoplanatic effects in the imagery.

Each restored image was translationally registered to the truth image to provide no penalty for a shift offset. The SSIM and MAE were calculated between the truth and restored image for the combinations of β = [0.1, 0.25, 1.0], α = [0, 0.5], and incorporating the interpolation blur for a bicubic interpolation used in the FIF restoration. The benefit to including the interpolation blur kernel in the FIF is captured in Table 3. SSIM and MAE both show lower error in the processed result with the interpolation blur PSF incorporated into the Wiener filter. Furthermore, the error metrics show how an increase in turbulence strength results in a lower quality restored image. The weaker turbulence case achieved a higher SSIM and lower MAE possible due to the turbulence providing a little more global shift to the imagery. The best β for the baseline and weak turbulence case was 0.25 as shown in Table 4. The alpha was not applicable for the baseline case as no turbulence was present in the imagery. The weak turbulence case appropriately optimized to the short exposure PSF per an α of 0.5.

Table 3: Error results solely focusing on interpolation blur PSF.

	Lighthouse				Houses			
	Interp PSF		No Interp PSF		Interp PSF		No Interp PSF	
Cn2	SSIM	MAE	SSIM	MAE	SSIM	MAE	SSIM	MAE
0.0	**0.556**	**9.703**	0.526	9.831	**0.617**	**12.537**	0.597	12.619
0.1e-15	**0.569**	10.051	0.557	**9.497**	**0.622**	**13.320**	0.485	15.660
0.9e-15	**0.397**	**11.661**	0.368	12.171	**0.468**	**16.039**	0.443	16.489
7.5e-15	**0.122**	**17.135**	0.117	17.253	**0.188**	**24.748**	0.180	24.974

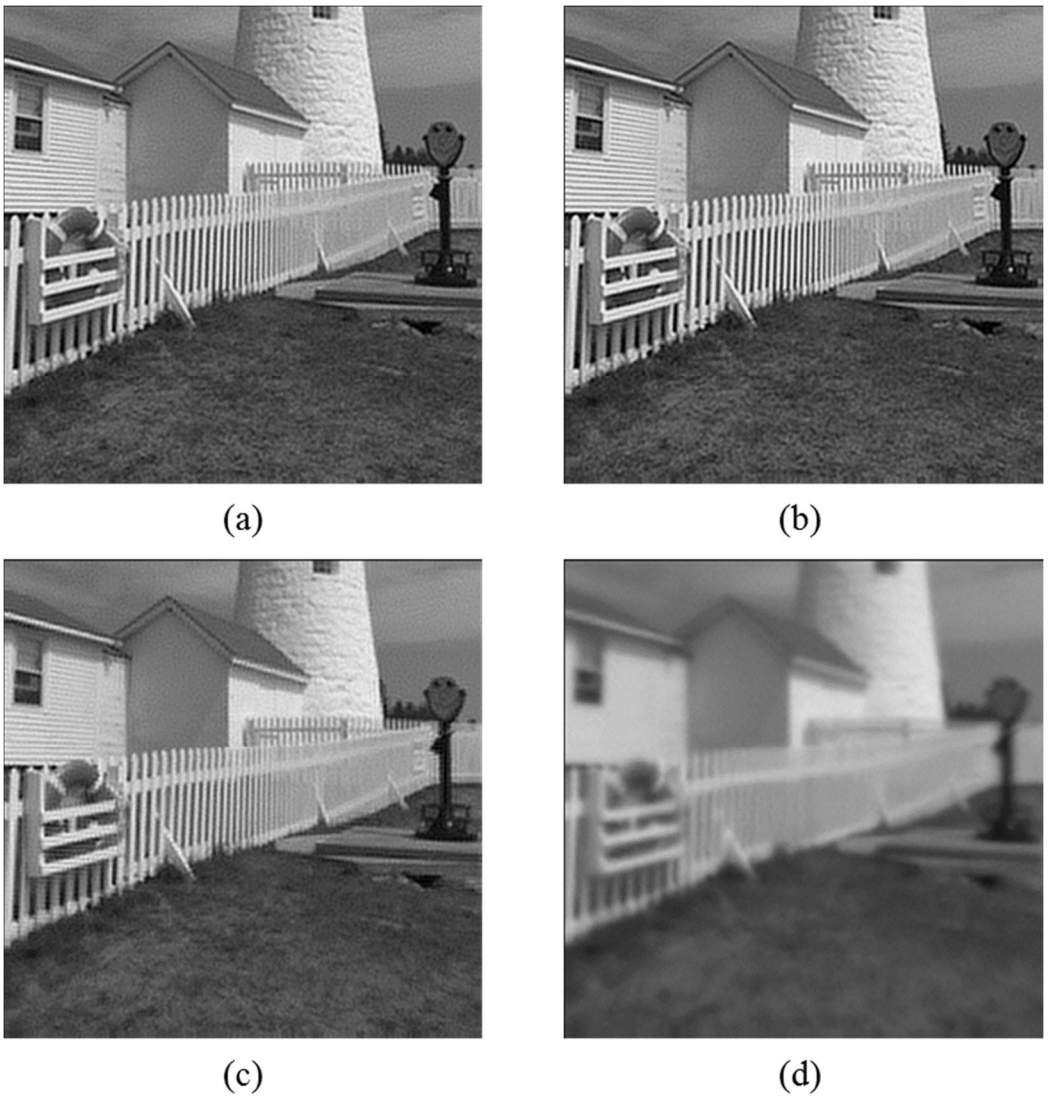

Figure 9. Restored output frames from the FIF. The baseline (a) is purely mitigating the effects of aliasing, while the light (b) and moderate (c) turbulence allow for the mitigation of both turbulence and aliasing. The heavy turbulence case (d) does not allow for any aliased frequencies to be recovered and thus provides a temporally averaged frame matching a long exposure observed frame with noise reduction.

Table 4: Best FIF parameter selection to minimize SSIM error.

	Lighthouse				House			
Cn2	β	α	NSR	SSIM	β	α	NSR	SSIM
0.0	0.25	N/A	0.0010	0.556	0.25	N/A	0.0010	0.617
0.1e-15	0.25	0.5	0.0014	0.569	0.25	0.5	0.0010	0.622
0.9e-15	0.25	0.5	0.0016	0.397	0.25	0.5	0.0015	0.468
7.5e-15	1	0.5	0.0058	0.122	1	0.5	0.0065	0.188

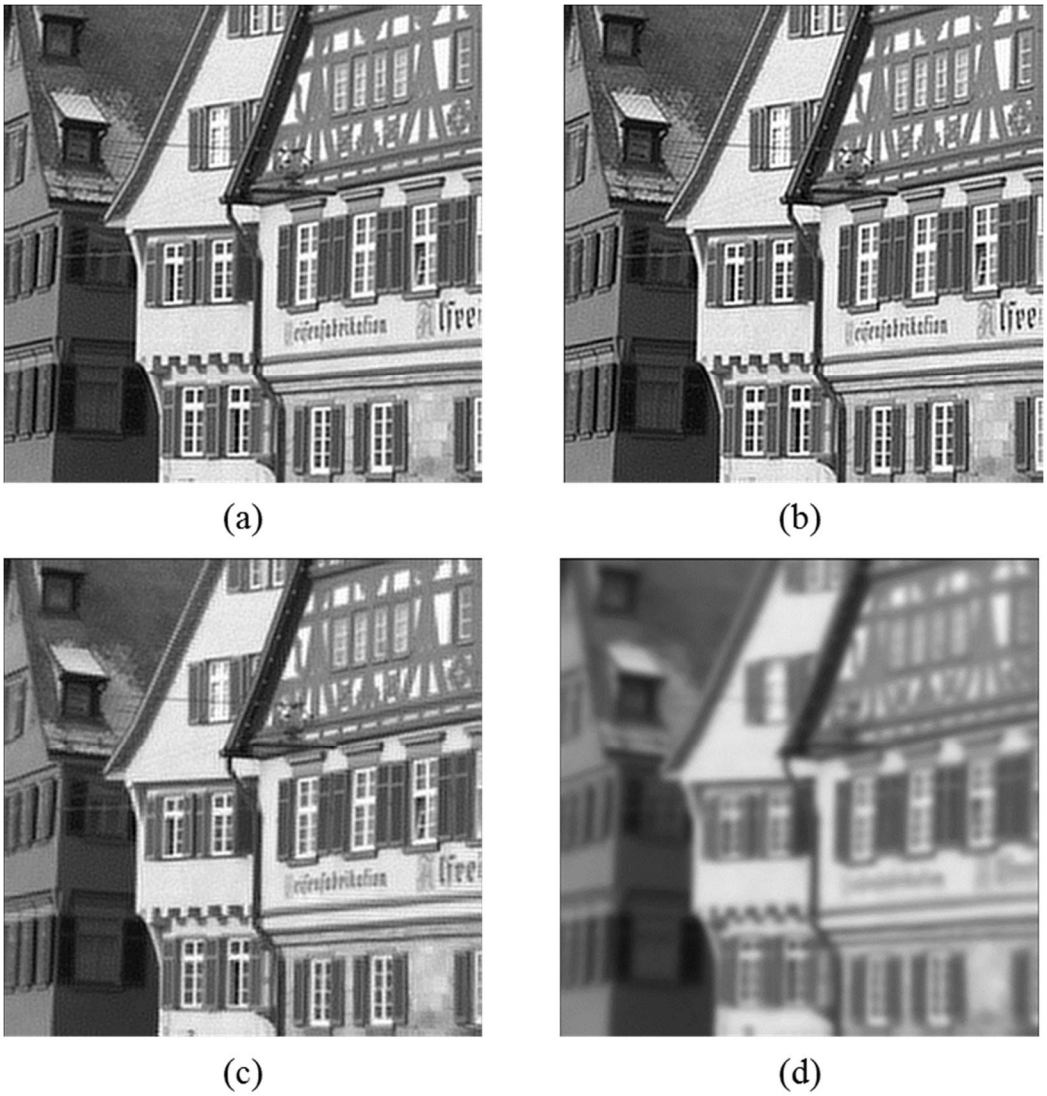

Figure 10. An additional set of restored imagery from the FIF algorithm for the same turbulence levels and camera parameters as Fig. 9.

Examining Figs 9 and 10, note that the baseline and weak turbulence restored images contain a lot of spatial frequency content that was aliased in the observed imagery. The siding on the side of the house, along with the fence posts match to the truth image. The moderate turbulence case does restore aliasing, is not as sharp. The lines in the siding on the house is weaker, along with the sign on the fence. The heavy turbulence case further reduces the sharpness of the image. The same can be true for the restored results of the houses shown in figure 10. The detail in the lettering on the side of the house becomes softer as the turbulence increases from moderate to heavy. Additionally, the roof shingles that were once aliased in the observed imagery are properly restored. Previous work[1] has shown how the registration, temporal averaging (β=1) and Wiener deconvolution still provides a sharper image than the long exposure image.

5. CONCLUSIONS

Our OTF analysis illustrates that scenarios certainly exist whereby imaging systems are impacted by optical turbulence, but still have aliasing due to undersampling. This will tend to happen under light to moderate turbulence. In heavy turbulence, the turbulence OTF acts as an anti-aliasing low pass filter. We suggest that the FIF SR method is well suited to addressing both the undersampling and the turbulence because its structure include temporal averaging, something critical to most TM methods. What makes the FIF SR particularly versatile is that this averaging is tunable with the parameter β. For high turbulence, a high β can be selected to provide straight temporal averaging. This effectively turns the FIF SR method into a traditional TM algorithm. On the other hand, a low β makes the fusion more selective and the FIF SR method more closely approximates a pure nonuniform interpolation SR method. Of course, options in between may be used to suit the level of undersampling and turbulence in a given application. An innovative aspect the proposed approach is that the Wiener filter is tuned to the level of registration, defined by α, and the level of interpolation blurring, defined by β. This increases the effectiveness of the Wiener filter.

6. REMARKS

This work was cleared for public release carrying the approval number 88ABW-2018-1656.

REFERENCES

[1] Hardie, R. C., Rucci, M. A., Dapore, A. J., and Karch, B. K., "Block matching and Wiener filtering approach to optical turbulence mitigation and its application to simulated and real imagery with quantitative error analysis," Opt. Eng. 56(7), 071503, doi: 10.1117/1.OE.56.7.071503 (2017)

[2] Fraser, D., Thorpe, G., and Lambert, A., "Atmospheric turbulence visualization with wide-area motion-blur restoration," *J. Opt. Soc. Am. A*, Vol. 16, No. 7, pp. 1751-1758 (July 1999).

[3] D. H. Frakes, J. W. Monaco, and M. J. T. Smith, "Suppression of Atmospheric Turbulence in Video Using an Adaptive Control Grid Interpolation Approach," *International Conference on Acoustics, Speech, and Signal Processing*. Salt Lake City, UT, USA, pp. 1881-1884 (2001).

[4] Hardie, R. C., Schultz, R. R., and Barner, K. E., "Super-resolution Enhancement of Digital Video," EURASIP JASP, Vol. 2007, Article ID 20984, (2007).

[5] Park, S. C., Park, M. K., and Kang, M. G., "Super-resolution image reconstruction: A technical overview," IEEE Signal Processing Mag. Vol. 20, Issue 3, pp. 21-36 (May, 2003).

[6] Hardie, R. C., Droege, D. R., Dapore, A. J., and Greiner, M. E., "Impact of detector-element active-area shape and fill factor on super-resolution," Frontiers in Physics: Optics and Photonics, https://doi.org/10.3389/fphy.2015.00031 (April 2015).

[7] Hardie, R. C., Barnard, K. and Ordonez, R., "Fast super-resolution with affine motion using an adaptive Wiener filter and its application to airborne imaging," OSA Optics Express, Vol. 19, Issue 27, 26208-26231 (2011).

[8] Mohamed, K. M. and Hardie, R. C., "A Collaborative Adaptive Wiener Filter for Multi-Frame Super-Resolution", Frontiers in Physics: Optics and Photonics, https://doi.org/10.3389/fphy.2015.00029 (April 2015).

[9] Karch, B. K. and Hardie, R. C., "Robust super-resolution by fusion of interpolated frames for color and grayscale images," Frontiers in Physics: Optics and Photonics, https://doi.org/10.3389/fphy.2015.00028A (April 2015).

[10] Yaroslavsky, L., Fishbain, B., Shabat, G., and Ideses, I., "Superresolution in turbulent videos: making profit from damage," *Optics Letters*, Vol. 32, No. 20, pp. 3038-3040 (Oct. 15, 2007).

[11] Fishbain, B., Yaroslavsky, L., and Ideses, I., "Spatial, Temporal, and Interchannel Image Data Fusion for Long-Distance Terrestrial Observation Systems," *Advances in Optical Technologies*, Vol. 2008, Article ID 546808, (2008).
[12] Droege, D. R., Hardie, R. C., Allen, B. S., Dapore, A. J. and Blevins, J. C., "A Real-Time Atmospheric Turbulence Mitigation and Super-Resolution Solution for Infrared Imaging Systems," Proceedings of SPIE Defense Security and Sensing, Baltimore, MD, USA (April 23-27, 2012).
[13] Hardie, R. C., Droege, D. R., Allen, B. S., Dapore, A. J., Blevins, J. C., and Hardin, K. M., "Real-Time Video Processing for Simultaneous Atmospheric Turbulence Mitigation and Super-Resolution and its Application to Terrestrial and Airborne Infrared Imaging," MSS Passive Sensors, Pasadena, CA, USA (March 2012).
[14] Fiete, R. D., "Image quality and λ FN/ p for remote sensing systems," *Optical Engineering,* Vol. 38, pp. 1229–1240 (1999).
[15] Goodman, J., [Introduction to Fourier Optics], McGraw-Hill, 1968.
[16] Roggemann, M. C., and B. Welsh, B., [Imaging Through Turbulence], CPC Press (1996).
[17] Hardie, R. C., Power, J. D., LeMaster, D. A., Droege, D. R., Gladysz S., Bose-Pillai S., "Simulation of anisoplanatic imaging through optical turbulence using numerical wave propagation with new validation analysis," Opt. Eng. 56(7), 071502, doi: 10.1117/1.OE.56.7.071502 (2017).